16
Quantum Transition State for Peptide Bond Formation in the Ribosome

Lou Massa, Chérif F. Matta, Ada Yonath, and Jerome Karle

16.1
Introduction

Crystallography is the principal method used to determine the structure of a ribosome, and consequently for understanding its functions, including formation of the peptide bond by ribozyme catalysis, and the decoding of the genetic code [1–5]. As shown in Figure 16.1, the ribosome is made of two subunits. It was found that the mRNA is decoded at the small subunit. The peptide bond is formed on the larger subunit within a cavity, hosting the peptidyl transferase center (PTC), composed mainly of ribosomal RNA [1–8].

Of importance to the quantum calculations reviewed in this chapter, a region of "pseudo twofold symmetry," which was detected in all known ribosome structures in and around the PTC [1,3b,3c,3d,3e], is associated with the translocation of the aminoacylated tRNA through the ribosome, as peptide bond formation occurs [2, 3], navigated by the ribosome architecture (Figure 16.2). The nascent proteins move out of the ribosome via an exit tunnel whose opening lies adjacent to the PTC and receives thereby each successive peptide bond as the protein elongates. Thus the architecture of the ribosome is consistent with the requirements of peptide bond catalysis and protein formation [2, 3, 5, 9, 10].

Given the structural architecture of the ribosome, quantum crystallography (QCr) [11] may be applied to study the transition state (TS) for peptide bond formation. (The foundations and applications of QCr are reviewed in Chapter 1.) QCr combines crystallographic structural information with quantum mechanical theory. This facilitates theoretical calculations and adds an energetic aspect to crystallography. The crystallographic structure is a starting point, constraint and anchor for the quantum calculations. In QCr the molecular system is mathematically divided into computationally tractable pieces. Subsequently, this may be followed by a quantum investigation of their mutual interactions, and thus in a step-by-step manner one may rebuild the entire quantum mechanism as a whole. This approach has been applied to the investigation of the peptide bond TS. The first step here was to

Quantum Biochemistry. Edited by Chérif F. Matta

ISBN: 978-3-527-32322-7

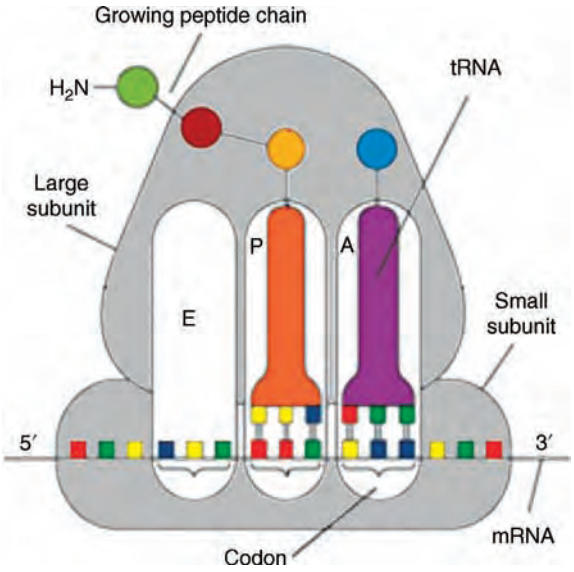

Figure 16.1 Protein synthesis [6]. Production line during protein synthesis, incoming tRNA (purple) carrying the next amino acid (blue circle) enters the A site if its anticodon (three "teeth" on its bottom) is complementary in sequence to the codon on mRNA. The reaction (not shown) between A-site tRNA and P-site tRNA (orange) extends the peptide chain by one amino acid unit. (Reproduced with the permission of the American Chemical Society from Reference [6].)

choose those atoms most likely to be importantly involved in the mechanism of peptide bond formation. This choice is small enough to be rigorously treated in density functional theory (DFT) quantum mechanics, but presumably large enough to represent the TS mechanism of peptide bond formation in the ribosome. Of course, this first choice can be successively expanded in future investigations.

A quantum mechanical TS for formation of the peptide bond has been found [12]. It is characterized by means of geometry, activation energy, thermodynamic parameters and quantum topology. The relevance of all this to peptide bond formation in the ribosome is discussed.

16.2
Methodology: Searching for the Transition State and Calculating its Properties

In this work, the Kohn–Sham equations of DFT were used to obtain the transition state for the peptide bond formation within the ribosome. The calculations included those 50 atoms assumed to be essential to peptide bond formation in the ribosome. Quantum mechanical calculations were carried out with the Mulliken program package [13]. The Becke three-parameter-hybrid (B3) [14] was used in conjunction with the Lee–Yang–Parr (LYP) functional [15] in all calculations, and a gaussian-type

Figure 16.2 Schematic indication of the combined linear and rotational motions associated with the movements of the aminoacylated tRNA through the ribosome. The twofold axis, shown in red, points towards the exit tunnel through which the elongating proteins escapes the ribosome. The apparent overlap of the two tRNA stems is a result of the specific view chosen to show best the concerted motions. (Reproduced with the permission of the National Academy of Science of the United States of America from Reference [12].)

basis set, 6-31+G(d,p) was used. In this manner, geometries of all reactants, products and transition states have been optimized at the DFT-B3LYP/6-31+G(d,p) level of theory.

Harmonic vibrational frequencies have been calculated using the same approximation for characterization of the nature of stationary points and zero-point vibrational energy (ZPVE) corrections. All the stationary points have been positively identified as minima with no imaginary frequencies, and the TS as a saddle point on the energy surface with one imaginary frequency. The bonds that are at the point of making and breaking in a transition state structure are consistent with a transformation connecting the desired reactants and products associated with peptide bond formation. The Cartesian coordinates of all atom positions in the optimized TS and calculated values of the vibrational frequencies are provided in Reference [12].

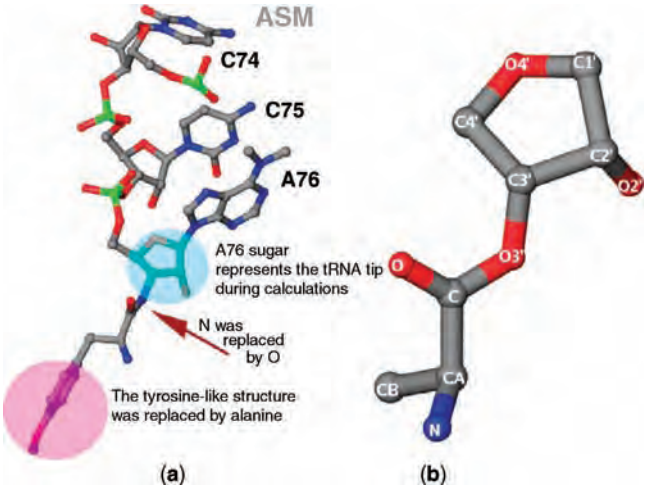

Figure 16.3 The 3′-end of the tRNA analog. (a) Tip of the tRNA ASM taken from the experimental crystal structure of its complex with D50S (Protein Data Bank ID code 1NJP), as used for the quantum mechanics calculations. The modified regions are highlighted by cyan and magenta. Hydrogen atoms are not shown. (b) Sugar moiety at tip of tRNA, charged with alanine. (Reproduced with the permission of the National Academy of Science of the United States of America from Reference [12].)

The crystal structure of a 50S large ribosomal subunit from *Deinococcus radiodurans* complexed with a tRNA acceptor stem mimic (ASM) was used ([2], 1NJP in Protein Data Bank). Figure 16.3a shows a small part of this structure, the 3′ end of the aminoacylated tRNA analog (ending with the highlighted sugar ring) attached via nitrogen to a tyrosine-like molecule (taking advantage of the non-hydrolysable nitrogen of the tRNA 3′end analog, puromycin). Because, in protein synthesis, amino acids attach to tRNA via ester-type bond we replaced N with an O at that location in the image shown. The highlighted region of the image contains atoms that have been judged to be of importance to the formation of the peptide bond. There are two analogous sets of such atoms, one is located in the A-site of the PTC and the other in the P-site, which was derived from A-site tRNA by rotation around the twofold axis. Both sets together constitute the 50 atoms chosen to represent the formation of the TS.

As shown in Figure 16.3a and b (hydrogen atoms not shown), we used the sugar moiety to represent the tip of tRNA, to investigate the actual reaction and, because of computational considerations, replaced the tyrosine-like bound amino acid structure with an alanine.

The TS results from a search that, except for initial conditions, is an automatic search, which only stops at a convergence satisfying stringent mathematical criteria. That occurs for a geometry that is at an energy minimum for every direction of displacement except one, for which it is at an energy maximum along a displacement toward products and away from reactants. A TS is a saddle point on the potential

energy surface, at which there occurs exactly one imaginary vibrational frequency, with all others real. The DFT quantum computations allow all 50 atoms to move freely, until a mathematically well-characterized TS is found. In terms of corroborating a TS, the bonds that are "making" and "breaking" must be consistent with the chemistry of the reaction.

The geometry of the TS, together with the twofold symmetry of the PTC [2, 3, 5, 10], has been used to estimate the angle of rotation of the A-site tRNA at the point of peptide bond formation. We made the estimate of rotation to the point of peptide bond TS formation by using coordinates of simulated ASM rotation every 15° about the twofold axis of the PTC. Superimposing our TS sugar moiety corresponding to the A site onto the acceptor stem mimic (ASM) sugar moiety, we let the TS ride around the twofold axis, looking for an angle that brought the second sugar moiety of the TS into best coincidence with its analog ring at the P site. We assumed that the position of the tRNA at the P-site is fixed, and it is the motion of the A site tRNA in its swing about the twofold axis that brings the reacting amino acids into coincidence. At each 15° increment of rotation we optimized the superposition of a TS sugar moiety onto that of the A site. In an analogous way we optimized a superposition of the TS sugar moiety onto that of the P site. Because the 50 atoms of the TS have been optimized independently of the tRNAs at A and P sites, it is not possible for the TS to fit them both simultaneously. Thus, we defined a best "average" position of the TS as occurring at the midpoint along a linear transformation between the optimal superpositions on the A and P sites. Using an objective error measure method [12], based upon the distance between analogous atoms at the average position of the TS and the A and P sites, we found the best match of our TS to the positions of the A and P sites to occur at a rotation angle of approximately 45°.

The thermodynamic parameters of the reaction that leads to TS in the ribosome have been measured in experiments. The corresponding parameters have been estimated for our theoretical TS, and they are found to be in qualitative proximal agreement with the experimental results [16].

A particular hydrogen atom, originally attached to the nitrogen of the A-site amino acid, has been suggested to participate in a "shuttle mechanism" (referenced below) during peptide bond formation. To study this proposed mechanism we carried out a topological study with methods of the quantum theory of atoms in molecules (QTAIM) (referenced below). Using the optimized geometry of the transition state [12], the Kohn–Sham (KS) [17] density functional theory (DFT)-B3LYP/6-31+G(d,p) level [14, 15] was used to define the origin of the intrinsic reaction coordinate axis (IRC) [18, 19]. The IRC is defined as "the minimum energy reaction pathway (MERP) in mass-weighted Cartesian coordinates between the transition state of a reaction and its reactants and products" [20]. (Gaussian 03 [21] was used in all electronic structure calculations.)

The evolution of the reaction was followed along the paths of steepest descent from the saddle point on both sides leading to the reactants and products, respectively. The initial direction of descent from the TS was that of the vibrational mode exhibiting an imaginary frequency. The reaction path was calculated without geometrical constraints using the algorithm of Gonzalez and Schlegel [22, 23]

sampling the path at 15 points on each side of the barrier at steps of 0.1 $amu^{1/2}$ bohr. Single point calculations were performed using 31 optimized geometries along the IRC (15 before and 15 after the TS in addition to the TS geometry). The resulting KS electron densities were subsequently analyzed according to the QTAIM [24–26] using the automated Windows implementation of AIMPAC [27, 28], AIMALL (T.A. Keith, personal communication 2009) and AIM2000 ([29–31]). The Poincaré–Hopf topological relationship [23] was verified for all points on the potential energy surface to ensure that no critical point had been missed.

16.3
Results: The Quantum Mechanical Transition State

Figure 16.4 shows the image of the optimized TS geometry for the formation of the peptide bond in the ribosome, including key geometrical parameters. The optimized TS bond distances are labeled according to whether they are in the act of breaking or forming, to achieve the transition from reactants to products. The end result is that the peptide bond N−C is formed, which results in elongating the nascent protein attached to the rotating A-site tRNA. The new O−H bond that is formed on the P-site tRNA saturates the open valence of the oxygen atom, which would occur as the C−O

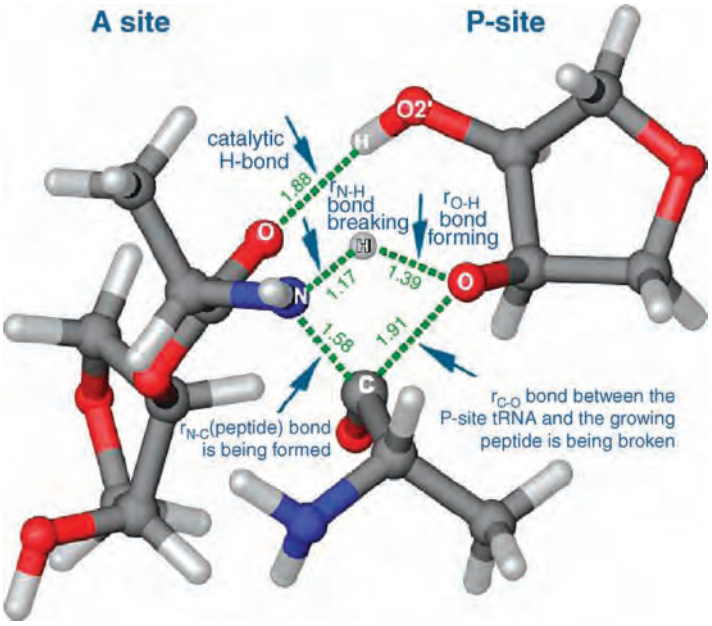

Figure 16.4 Peptide bond transition state in the ribosome. The amino acids are alanine. (Reproduced with permission of the National Academy of Science of the United States of America from Reference [12].)

bond breaks to allow release of the amino acid transferred to the nascent protein. A bond that is breaking in the TS, namely, N−H, completes the release of the P-site tRNA. Hence, given such bond making and breaking, the former A-site tRNA can occupy the P-site which becomes available by the former P-site tRNA release.

The TS geometry of Figure 16.4 shows the 2′OH of the P-site forming a hydrogen bond with the carboxyl oxygen of the A-site amino acid. That hydrogen bond is formed in the TS, having a bond length 1.879 Å. Such hydrogen bonding, perhaps serving as an anchor holding reactants in place at the TS, is consistent with the catalytic role that has been ascribed to the tRNA A76 2′OH group based on biochemical experiments [9]. Careful examination of Figure 16.4, which conveys something of the three-dimensional arrangements of the atoms in the TS, allows one to perceive how the peptide bond is being formed, and how the P site tRNA is allowed to break away after the peptide bond is being made.

Our TS has a calculated activation energy, E_a, of 35.5 kcal mol^{-1} (1 kcal = 4.184 kJ). However, we found that in the ribosome the number of hydrogen bonds, between the rotating moiety of the tRNA aminoacylated 3′end and the surrounding nucleotides of the PTC, increases as the reactants move toward the transition state, resulting in lower activation energy. The number of hydrogen bonds, based upon a distance criterion that considers a hydrogen bond "cut off" at 4 Å, as a function of the angle of rotation about the twofold axis of symmetry in the PTC shows an increase of three hydrogen bonds as the transition state forms [12]. Assuming, on qualitative grounds, that such hydrogen bonds might vary in strength over the range 2–10 kcal mol^{-1} [32], an average value of 6 kcal mol^{-1} is adopted for each of the three newly formed hydrogen bonds. This implies a net stabilization of 18 kcal mol^{-1} that would reduce the calculated activation energy to a qualitatively estimated value of approximately 18 kcal mol^{-1} (Table 16.1).

The amino acids that are the reactants in the TS reaction are attached to large tRNA molecules, which suppress their translation and rotation degrees of freedom. The electronic levels are assumed to be too widely spaced to contribute to entropy change. Therefore, we take the electronic, translational and rotational contributions to entropy to be zero [16]. Consequently, the conditions of the ribosome environment reduce the change of entropy to that associated only with the vibrational degrees of freedom; that is, only the vibrational frequencies of the normal modes at the optimized geometries for the TS and reactants are required to obtain the entropies. These have been obtained using the Gaussian program package [21]. For the non-catalyzed reaction the calculated entropy contribution to the free energy change is $T\Delta S^{\ddagger}_{\text{total}} = -14.6$ kcal mol^{-1}, corresponding to an enormous and unfavorable decrease in entropy [16]. This may be compared to the catalyzed reaction in which the TS is stabilized by the formation of three hydrogen bonds to the ribosome nucleotides, and in which the translational and rotational degrees of freedom are suppressed by the ribosome. In this case the estimated overall entropy contribution to the free energy change is $T\Delta S^{\ddagger}\text{v}_{\text{ib}+3\text{HB}} = 1.5$ kcal mol^{-1}, which corresponds to a favorable increase in entropy [16]. The calculated enthalpy changes ($\Delta H^{\ddagger}$) for the non-catalyzed and catalyzed reactions are known from previous work [12, 16] to be 34.3 and 16.3 kcal mol^{-1}, respectively. These enthalpies are obtained from the corresponding

Table 16.1 Calculated energies (using B3LYP/6-31+G(d,p) method) along the peptide bond formation pathway.[a)]

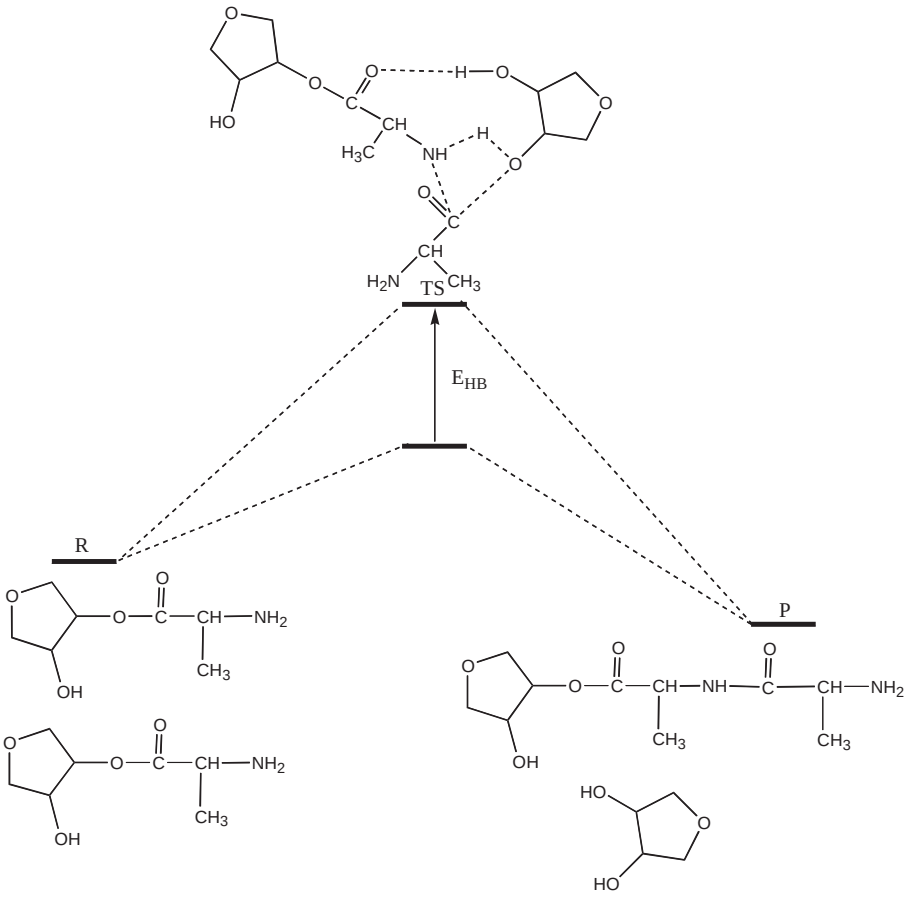

Chemical species	Energy (au)	Relative (to reactants) energy (kcal mol^{-1})
R	−1259.78 590	0.0
TS	−1259.72 318	35.5
P	−1259.79 099	−3.2

a) ΔE_{HB} represents the qualitative reduction in our calculated transition state activation energy that would be expected to occur because of increased hydrogen bonding concomitant with the reaction's progress towards the transition state. An increase of three hydrogen bonds, of average magnitude 6 kcal mol^{-1}, would be consistent with a qualitatively estimated transition state barrier of 18 kcal mol^{-1}. (Reproduced with the permission of the National Academy of Science of the United States of America from Reference [12].)

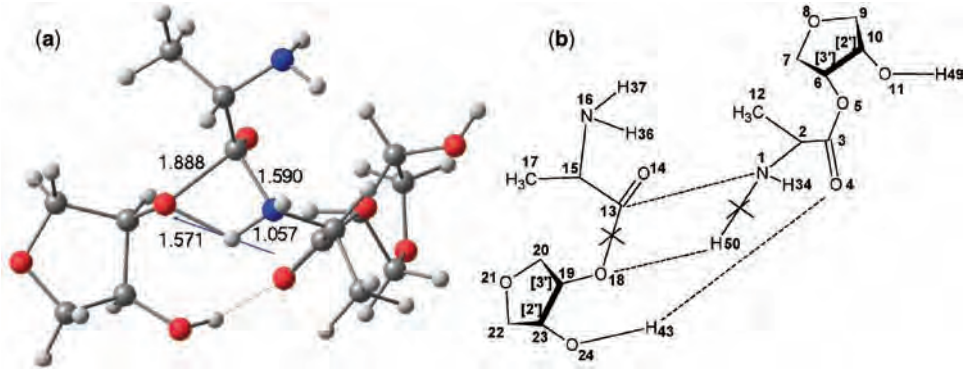

Figure 16.5 (a) Ball-and-stick model of the transition state with an arrow representation of the eigenvector of the single imaginary frequency ($\nu_{im} = -1084.13i\,cm^{-1}$). The arrow clearly indicates the transfer of hydrogen from the amine nitrogen to the oxygen O3′ (O18) of the P-site ribose sugar. The O2′ hydroxyl group of the P-site tRNA (O24−H43) forms a stable hydrogen bond, indicated by a dashed line, to the ester carbonyl group of the tRNA at the A-site (O4). (b) Diagram of the TS, showing the atom numbering scheme adopted in the discussion.

calculated activation energies E_a, which are 35.5 and 17.5 kcal mol^{-1}, respectively. Thus, the TS reaction within the ribosome is enhanced by both enthalpy and entropy relative to what would be the case for the same reaction in the gas phase. As regards entropy, its identification with noise allows the conclusion that the ribosome, by suppressing noise, contributes to catalysis of the peptide bond.

As can be seen from Figure 16.5, the eigenvector associated with the imaginary frequency ($\nu_{im} = -1084.13i\,cm^{-1}$, in the harmonic approximation) is centered on H50, the hydrogen atom being transferred from the $-NH_2$ (−N1-H50-H34) to O3′ (O18) of the P-site ribose sugar. This vector points in the direction of the reaction path when the system is at the TS point on the PES, which clearly indicates the transfer of H50 from the amine nitrogen to the oxygen. Figure 16.5 also provides the interatomic distances of the bonds that are forming (C−N and O−H) and breaking (N−H and O−C).

Figure 16.6 displays the molecular graph (the collection of bond paths) of the TS along with the number and type of critical points that satisfy the Poincaré–Hopf relationship. The lines of maximum electron density linking the (bonded) nuclei are the bond paths and the saddle points on those paths, indicated by the small red dots, are the bond critical points (BCPs). The yellow dots are the ring critical points. Each nuclear critical point is color-coded in the figure to reflect the identity of the atomic element. The Poincaré–Hopf relationship is (Equation 16.1):

$$n_{NCP} - n_{BCP} + n_{RCP} - n_{CCP} = 1 \tag{16.1}$$

where n_{NCP} is the number of nuclear critical points (50, in total), n_{BCP} the number of bond critical points (56), n_{RCP} the number of ring critical points (7) and n_{CCP} the number of cage critical points (none were found in the molecular graph of the TS).

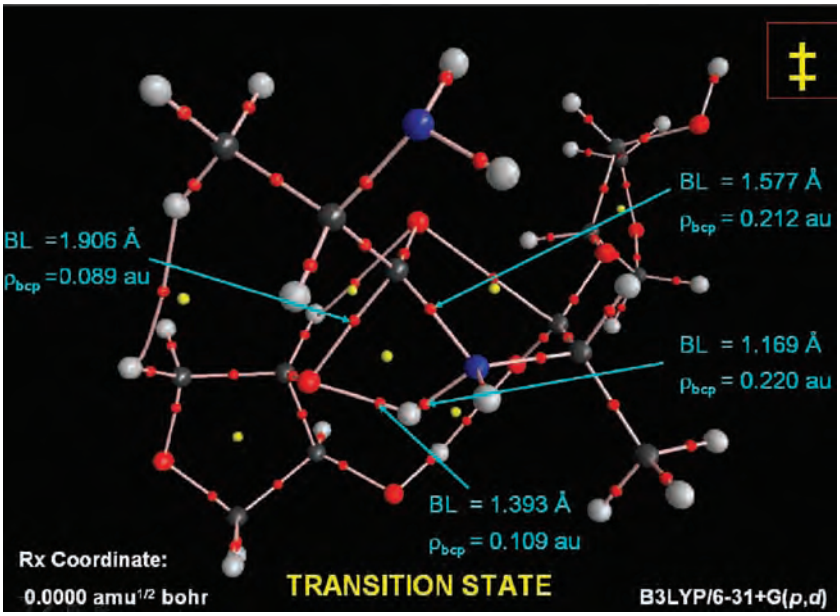

Figure 16.6 Molecular graph of the transition state. The large dark spheres indicate the nuclear critical points of carbon atoms, the large red sphere those of the oxygen nuclei, the blue spheres nitrogen nuclei and the large light gray spheres indicate the position of the hydrogen nuclear critical points. The lines of maximum electron density linking the (bonded) nuclei are the bond paths and the saddle points on those paths, indicated by the small red dots, are the bond critical points (BCPs). The yellow dots are the ring critical points. (BL stands for "bond length." The Poincaré–Hopf relationship (Equation 16.1) is satisfied by the molecular graph (n_{NCP} (50) − n_{BCP} (56) + n_{RCP} (7) − n_{CCP} (0) = 1).

The molecular graph in Figure 16.6 satisfies the Poincaré–Hopf relationship. In Figure 16.6 attention is drawn to the lines of maximum electron density linking the nuclei. These bond paths connect the hydrogen atom (H50) referred to in the shuttle mechanism to the oxygen O3′, and *not* to oxygen O2′. This same bond path connection is preserved for all 15 points that have been calculated along the IRC beyond the TS moving towards products. The TS we characterized and the sequence of bond paths making and breaking precludes a shuttle mechanism in the present Ala-Ala system, and supports direct mechanism described above. Consistent with this, Figure 16.6 shows that the O2′ hydroxyl group of the P-site tRNA (O24−H43) exhibits a bond path indicative of a hydrogen bond to the ester carbonyl group of the tRNA at the A-site (O4). The estimated energy of this hydrogen bond from the Espinosa–Molins–Lecomte (EML) empirical topological formula [33] is around 7 kcal mol^{-1} and remains constant in the segment of the reaction path we have studied. Its role appears to be to hold the reacting system in place for optimum orientation of the reacting groups. This hydrogen bond would be broken at later stages along the reaction path for the A-site and P-site reacting fragments to detach after formation of the peptide bond.

16.4 Discussion

The potential energy surface of 50 atoms considered to be most important in peptide bond formation has been calculated. Within the quantum mechanics of DFT (B3LYP) we have computed a molecular structure and energy that satisfies the mathematical criteria for a TS, including a frequency spectrum with all but one frequency real. The TS makes good chemical sense, in terms of what the amino acid molecules must do, namely, form a peptide bond, attach an elongating peptide to A-site tRNA as it moves to P-site, and have P-site tRNA separate from A-site tRNA. The chemical sense, after the mathematical criteria, is what corroborates the TS.

The calculated E_a of 35.5 kcal mol^{-1} for our TS applies only to the barrier associated with those 50 atoms considered in the DFT calculation. However, qualitative considerations make clear how such an activation energy would be stabilized in the ribosome. During elongation the A-site tRNA carries out a "linear motion." At the same time its 3′end, namely the amino acid attached to its CCA end, executes a rotational twofold motion. The combined linear and rotational motions of the full tRNA are indicated schematically in Figure 16.2. The number of hydrogen bonds associated with the rotating moiety of the tRNA 3′end within the PTC appears to increase by as much as three hydrogen bonds between 0 and 45° [12]. Adopting a reasonable average energy for such hydrogen bonds allows a qualitative estimate of the stabilization of the transition state that would occur. If every hydrogen bond confers $\sim$ 6 kcal mol^{-1}, three such bonds would confer 18 kcal mol^{-1} of stabilization. Thus, a qualitative estimate for the activation energy barrier for formation of the peptide bond in the ribosome would be approximately 18 kcal mol^{-1}. This qualitative estimate for the approximate E_a may be compared to the related (but different) experimental measurement [34], which has $E_a = 17.5$ kcal mol^{-1}; see also the related theoretical calculations of [35–37], all of which, however, deal with mechanisms different than our own.

Interestingly, the TS geometry is achieved after a modest rotation, which we estimate as 45°. At that stage the P-site O2′ hydroxyl group forms a hydrogen-bond within the TS. Such an H-bond can stabilize the TS geometry, as recently suggested by biochemical studies [38]. This means that the TS for the peptide bond is made rather early in the rotation. However, the final bonds made and broken that result from the TS will achieve their equilibrium values after further rotation along the guiding reaction pathway associated with the twofold axis of the PTC.

We conclude that it is satisfactory that the DFT quantum computations, allowing all 50 atoms to move freely, have found a mathematically, well-characterized TS. In addition, the fact that the OH group at the P site ends up making a catalyzing hydrogen bond, in accordance with experiments that are generally agreed to be credible, underlines again the chemical sense our TS conveys.

The non-catalyzed reaction of the amino acids we have considered is associated with an enormous and unfavorable decrease in entropy related to translation and rotation degrees of freedom. However, in the ribosome these degrees of freedom are suppressed, by the tRNA attachments to the reactant amino acids, and because of

that suppression the catalyzed reaction shows a favorable increase in entropy [16]. Using the gas-phase non-catalyzed reaction as a standard of comparison, the ribosome environment enhances the formation of the peptide bond from both an enthalpy and an entropy point of view. The activation energy for formation of the TS is reduced by formation of three external hydrogen bonds. The entropy is increased by the suppression of translational and rotational degrees of freedom. The remaining vibrational degrees of freedom contribute to an increase of entropy. This is counteracted by a decrease of entropy associated with the formation of three hydrogen bonds. On balance, there remains an overall increase of entropy as the TS is formed. Both enthalpy and entropy contribute to ribosome amino acid reaction catalysis.

A so-called "proton shuttle" mechanism [36, 37] has been suggested in the ribosome literature. As may be seen in Figure 16.4, once the C−O bond is broken, between the P-site sugar and the growing peptide, the valence of the oxygen atom, that is O3′, remains to be satisfied by bonding to a hydrogen atom. The proton shuttle proposal is one that entails the amino hydrogen from the A-site being passed over to the P-site O2′ oxygen, which passes its own hydrogen within the P-site for valence satisfaction of its O3′ oxygen. But with regard to our quantum mechanical TS, the shuttle mechanism is precluded. As shown in Figure 16.5, the vibrational motion of the amino hydrogen projects it directly towards the P-site O3′, and away from O2′. Moreover, quantum topological arguments inveigh against the shuttle mechanism for the TS, as indicated in Figure 16.6, which shows the molecular graph for the TS. At equilibrium the molecular graph is made up of bond paths, that is, universal indicators of which atoms are bonded to one another [39]. Other than for geometries at stationary points on the potential energy surface [e.g., equilibrium geometries or first-order saddle points (TS)] these lines are called atomic interaction lines. A bond path is a ridge of electron density linking chemically-interacting nuclei and contributing to the stability (i.e., lowering) of the electronic potential energy for any nuclear configuration, at equilibrium or not. Consequently, the ridge of maximal density is the line along which the density contributes maximally to electronic potential energy stability. Following the TS, in the direction of the final chemical products, before a new equilibrium geometry is reached, a bonding interaction must develop along the reaction path (the IRC) that is indicative of the direction in which equilibrium lies. There is a continuity of meaning for atomic interaction lines and bond paths. If at a stationary point geometry there is to be a bond path between nuclei, its precursor is an interaction line that develops along the IRC. As regards the shuttle mechanism in the ribosome TS of Figure 16.6, the interaction line that develops along the IRC is the quantum topological definitive proof that there is no shuttle mechanism. This is because the proposed shuttle is inconsistent with the molecular graph drawn by interaction lines along the IRC that follows the TS. Once beyond the TS, that is for all 15 IRC energy calculations we have examined for this reaction, there is a consistent atomic interaction line between the amino hydrogen and the P-site O3′ analogous to that shown in Figure 16.6 at the TS. Such a line connecting to the P-site O2′ would be required for the shuttle mechanism to hold, but no such line occurs. Moreover, the O2′ hydroxyl group of the P-site tRNA (O24−H43) exhibits a remarkably stable hydrogen bond path to the ester carbonyl group of the tRNA at the

A-site (O4). The estimated energy of this hydrogen bond from the EML formula of Reference [33] is around 7 kcal mol^{-1} and remains constant in the segment of the reaction path we have studied explicitly. This too is inconsistent with a proton shuttle involving O2′. Instead, the role of the O2′ hydroxyl group appears to be, through formation of a hydrogen bond, to hold the reacting system in place for optimum reaction orientation. This hydrogen bond is broken at later stages along the reaction path to allow the for P-site tRNA to exit the ribosome. The mechanism presented here is simpler than the popular proton shuttle mechanism, inasmuch as it involves a direct transfer of hydrogen from the attacking $-NH_2$ group to the ester oxygen at the 3′ carbon of the P-site sugar.

16.5 Summary and Conclusions

Quantum mechanics and crystallography have been joined to study the formation of the peptide bond as it occurs in the ribosome's peptidyl transferase center (PTC). Quantum calculations were based upon a choice of 50 atoms assumed to be important in the mechanism. Density functional theory (DFT) was used to optimize the geometry and energy of the transition state (TS) for peptide bond formation. The calculated transition state activation energy, E_a, is 35.5 kcal mol^{-1}. However, an increase in hydrogen bonding occurs between A-site tRNA and ribosome nucleotides during the twofold rotation from the A-site towards the P-site as the TS forms. The activation energy is stabilized by the increase in hydrogen bonding to a value qualitatively estimated to be approximately 18 kcal mol^{-1}. The optimized geometry of the TS corresponds to a structure in which the peptide bond is being formed as other bonds are being broken, in just such a manner as to release the P-site tRNA so that it may exit as a free molecule, and be replaced by its A-site analog attached to an elongating nascent protein. The entropy increase of the TS is estimated. The calculated thermal parameters of the TS are in qualitative agreement with corresponding experimental values. At TS formation the 2′OH group of the P-site tRNA A76 forms a hydrogen bond with the oxygen atom of the carboxyl group of the amino acid attached to the A-site tRNA, suggestive of a catalytic role, which is consistent with experimental findings. The estimated magnitude of the rotation angle about the ribosomal twofold pseudo-symmetrical axis, between the A-site starting position and the place at which the TS occurs, is approximately 45°. Using quantum topology we investigated a "shuttle mechanism," which has often been suggested in the literature to describe hydrogen atom transfer associated with peptide bond formation. The inconsistency between this mechanism and the quantum mechanical transition state is discussed.

Acknowledgments

Thanks are due to Professor Richard F. W. Bader for suggesting that a QTAIM analysis would shed light on the nature of the TS. We acknowledge ribosome studies

in collaboration with Asta Gindulyte, Anat Bashan and Ilana Agmon, [12]. L.M.'s studies were funded by U.S. Army, breast cancer award, W81XWH-06-1-0658, US National Institute of Health (NIGMS MBRS SCORE 5S06GM606654) and the National Center for Research Resources (RR-03037). C.M. acknowledges the Natural Sciences and Engineering Research Council of Canada (NSERC), Canada Foundation for Innovation (CFI) and Mount Saint Vincent University for funding. A.Y. was supported by National Institutes of Health Grant GM34360, Human Frontier Science Program Organization Grant RGP0076_2003 and the Kimmelman Center for Macromolecular Assemblies. A.Y. holds the Martin and Helen Kimmel Professorial Chair. The research at The Naval Research Laboratory was supported by the Office of Naval Research. The authors thank the National Academy of Science of the United States of America and the American Chemical Society for permissions to reproduce copyrighted material.

References

1 Harms, J., Schluenzen, F., Zarivach, R., Bashan, A., Gat, S., Agmon, I., Bartels, H., Franceschi, F., and Yonath, A. (2001) *Cell*, **107**, 679–688.

2 Bashan, A., Agmon, I., Zarivach, R., Schluenzen, F., Harms, J., Berisio, R., Bartels, H., Franceschi, F., Auerbach, T., Hansen, H.A.S., Kossoy, E., Kessler, M., and Yonath, A. (2003) *Mol. Cell.*, **11**, 91–102.

3 (a) Agmon, I., Bashan, A., Zarivach, R., and Yonath, A. (2005) *Biol. Chem.*, **386**, 833–844; (b) Ban, N., Nissen, P., Hansen, J., Moore, P.B., and Steitz, T.A. (2000) *Science*, **289**, 905–920; (c) Schuwirth, B.S., Borovinskaya, M.A., Hau, C.W., Zhang, W., Vila-Sanjurjo, A., Holton, J.M., and Cate, J.H.D. (2005) *Science*, **310**, 827–834; (d) Selmer, M., Dunham, C.M., Murphy Iv, F.V., Weixlbaumer, A., Petry, S., Kelley, A.C., Weir, J.R., and Ramakrishnan, V. (2006) *Science*, **313**, 1935–1942; (e) Korostelev, A., Trakhanov, S., Laurberg, M., and Noller, H.F. (2006) *Cell*, **126**, 1065–1077.

4 Yonath, A. (2003) *Biol. Chem.*, **384**, 1411–1419.

5 Yonath, A. (2005) *Mol. Cell*, **20**, 1–16.

6 Borman, S. (2007) *Chem. Eng. News*, **85(8)**, 13–16.

7 Youngman, E.M., Brunelle, J.L., Kochaniak, A.B., and Green, R. (2004) *Cell*, **117**, 589–599.

8 Brunelle, J.L., Youngman, E.M., Sharma, D., and Green, R. (2006) *RNA*, **12**, 33–39.

9 Weinger, J.S., Parnell, K.M., Dorner, S., Green, R., and Strobel, S.A. (2004) *Nat. Struct. Mol. Biol.*, **11**, 1101–1106.

10 Bashan, A. and Yonath, A. (2005) *Biochem. Soc. Trans.*, **33**, 488–492.

11 Huang, L., Massa, L., and Karle, J. (2001) *IBM J. Res. Dev.*, **45**, 409–415.

12 Gindulyte, A., Bashan, A., Agmon, I., Massa, L., Yonath, A., and Karle, J. (2006) *Proc. Natl. Acad. Sci. U.S.A.*, **103**, 13327–13332.

13 IBM, MULLIKEN. MULLIKEN is IBM proprietary software package that implements *ab initio* quantum chemical calculations on the IBM SP/2 supercomputer (The Laboratory for Quantum Crystallography, Hunter College, CUNY) (1995).

14 Becke, A.D. (1993) *J. Chem. Phys.*, **98**, 5648–5652.

15 Lee, C., Yang, W., and Parr, R.G. (1988) *Phys. Rev. B*, **37**, 785–789.

16 Massa, L. (2007) Comment on the suppression of noise by the ribosome. The SPIE Symposium on Fluctuations and Noise, 20–24 May at the La Pietra Center in Florence, Italy.

17 Kohn, W. and Sham, L.J. (1965) *Phys. Rev. A*, **140**, 1133–1138.

18 Fukui, K. (1970) *J. Phys. Chem.*, **74**, 4161–4163.

19 Fukui, K. (1981) *Acc. Chem. Res.*, **14**, 363–368.

20 Zipse, H. (2008) Following the intrinsic reaction coordinate, http://www.cup.uni-muenchen.de/oc/zipse/compchem/geom/irc1.html.

21 Frisch, M.J., Trucks, G.W., Schlegel, H.B. *et al.* (2003) Gaussian 03, Gaussian, Inc., Pittsburgh, PA.

22 Gonzalez, C. and Schlegel, H.B. (1989) *J. Chem. Phys.*, **90**, 2154.

23 Gonzalez, C. and Schlegel, H.B. (1990) *J. Phys. Chem.*, **94**, 5523–5527.

24 Bader, R.F.W. (1990) *Atoms in Molecules: A Quantum Theory*, Oxford University Press, Oxford, UK.

25 Popelier, P.L.A. (2000) *Atoms in Molecules: An Introduction*, Prentice Hall, London.

26 Matta, C.F. and Boyd, R.J. (eds) (2007) *The Quantum Theory of Atoms in Molecules: From Solid State to DNA and Drug Design*, Wiley-VCH Verlag GmbH, Weinheim.

27 Biegler-König, F.W., Bader, R.F.W., and Tang, T.-H. (1982) *J. Comput. Chem.*, **13**, 317–328.

28 Bader, R.F.W. AIMPAC, http://www.chemistry.mcmaster.ca/aimpac/.

29 Biegler-König, F.W., Schönbohm, J., and Bayles, D. (2000) AIM2000, http://gauss.fh-bielefeld.de/aim2000.

30 Biegler-König, F.W., Schönbohm, J., and Bayles, D. (2001) *J. Comput. Chem.*, **22**, 545–559.

31 Biegler-König, F.W. (2000) *J. Comput. Chem.*, **21**, 1040–1048.

32 Lii, J.-H. (1998) in *Encyclopedia of Computational Chemistry* (ed. P.R. Schleyer), John Wiley & Sons, Ltd, pp. 1271–1283.

33 Espinosa, E., Molins, E., and Lecomte, C. (1998) *Chem. Phys. Lett.*, **285**, 170–173.

34 Sievers, A., Beringer, M., Rodnina, M.V., and Wolfenden, R. (2004) *Proc. Natl. Acad. Sci. U.S.A.*, **101**, 7897–7901.

35 Das, S.R. and Piccirilli, J.A. (2005) *Nat. Chem. Biol.*, **1**, 45–52.

36 Sharma, P.K., Xiang, Y., Kato, M., and Warshel, A. (2005) *Biochemistry*, **44**, 11307–11314.

37 Trobro, S. and Aqvist, J. (2005) *Proc. Natl. Acad. Sci. U.S.A.*, **102**, 12395–12400.

38 Huang, K.S., Weinger, J.S., Butler, E.B., and Strobel, S.A. (2006) *J. Am. Chem. Soc.*, **128**, 3108–3109.

39 Bader, R.F.W. (1998) *J. Phys. Chem. A*, **102**, 7314–7323.